Biol. Cybern. 71. 307–317 (1994)

Biological Cybernetics

The reaching task: evidence for vector arithmetic in the motor system?

A. David Redish, David S. Touretzky

School of Computer Science, Carnegie Mellon University, Pittsburgh, PA 15213, USA

Received: 9 September 1993/Accepted in revised form: 8 March 1994

Abstract. During a reaching task, the population vector is an encoding of direction based on cells with cosine response functions. Scaling the response by a magnitude factor produces a vector encoding, enabling vector arithmetic to be performed by the summation of firing rates. We show that the response properties of selected populations of cells in the primary motor cortex and area 5 can be explained in terms of arithmetic relationships among load, goal, and motor command vectors. Our computer simulations show good agreement with single-cell recording data.

1 Introduction

1.1 The task

For more than a decade, researchers have conducted variations of the following experiment involving monkeys (usually macaques). Eight light-emitting diodes (LEDs) are arranged at equidistant points on a circle in front of the animal, with a ninth LED in the center. The monkey is trained to select (by pointing or by maneuvering a manipulandum) the LEDs while single-cell recordings are made. A trial begins when the center LED is lit, and the monkey selects it. After a delay, one of the peripheral LEDs is lit, and the monkey selects the lit LED. (See Georgopoulos et al. 1983 for the original definition of this task.)

Many variations of this task have been studied. In isometric versions, the LED board is replaced with a video monitor, and the monkey selects the lights via a fixed, force-sensitive joystick (Georgopoulos et al. 1992). In three-dimensional versions, the LEDs are replaced by eight lighted pushbuttons arranged at the corners of a cube in space in front of the monkey, with a ninth pushbutton at the center (Schwartz et al. 1988; Caminiti et al. 1990a, b, 1991). Schwartz (1992, 1993) even reports a variation of this task in which a monkey was trained to trace sinusoids of varying widths and frequencies with its finger.

We will concentrate on one variant of the reaching task in which a static load is attached to the manipulandum in such a way that the load vector can be applied in any of eight directions (Kalaska et al. 1989, 1990; Kalaska 1991) (Fig. 1). This allows the dissociation across trials of the intended motion or 'goal' direction from the direction in which the monkey actually has to exert force in order to reach the goal. In discussing this task, we will refer to the intended motion direction of the hand as the 'goal vector' $\vec{G}$, and the actual force exerted as the 'motor command' $\vec{M}$. We will refer to the 'load vector' imposed (expressed in hand coordinates) as $\vec{L}$.

1.2 The data

Our model addresses data relating subpopulations of three areas of the motor system: the dorsal premotor area (PMd), primary motor cortex (MI), and superior parietal cortex (area 5). In general, activity in the premotor cortex precedes activity in the motor cortex, which in turn precedes activity in area 5 (for a review see Kalaska and Crammond 1992).

Neurons in shoulder-related areas of PMd have been recorded whose firing rate covaries with the direction of the goal vector $\vec{G}$ (Caminiti et al. 1990a, 1991), while some neurons in shoulder-related areas of MI and area 5 have firing rates the covary with the directions of both $\vec{G}$ and $\vec{L}$ (Kalaska et al. 1989, 1990). In all three cases, the firing rates of these neurons correlate closely with a cosine function of the vector direction. This allows the definition of a *preferred direction* of a neuron as the peak of the cosine function.

The *goal axis* of the neuron is defined as the preferred direction with respect to $\vec{G}$ and the *load axis* as the preferred direction with respect to $\vec{L}$. Although individual neurons in both the MI and area 5 populations show goal and load responses, in the MI population the goal and load axes are anti-correlated (left half of Fig. 4), while in the area 5 population the goal and load axes are uncorrelated (left half of Fig. 5).

Although PMd shoulder-related neurons have not been recorded during the loaded reaching task, in other

Correspondence to: D. S. Touretzky

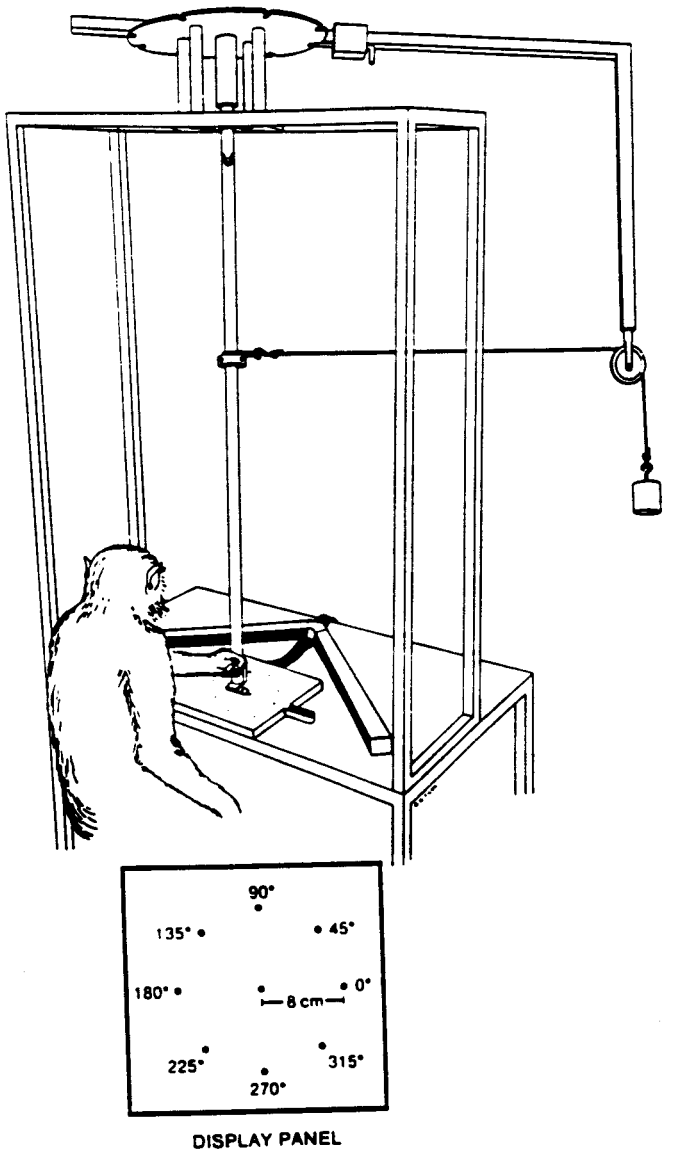

Fig. 1. The experimental setup for the loaded reaching task (from Kalaska et al. 1989, used with permission of the author and publisher)

tasks they have been shown to be less likely to be sensitive to variations in force than MI neurons (Werner et al. 1991).

The evidence from the motor cortex is inconsistent. Many researchers have reported a strong correlation between the firing rates of tonic motor cortex neurons and static force (see Hepp-Reymond 1988 for a review). This correlation is sigmoidal, with a large linear range (Cheney and Fetz 1980; Evarts et al. 1983; Kalaska 1991). However, a recent experiment by Georgopoulos et al. (1992) has shown that in the absence of movement, some shoulder-related MI neurons do not show a relation to static force; they respond only to dynamic force. We do not know of a way of reconciling the differences between this latest result and the previous work. However, Wise (1993) points out that Georgopoulos et al. looked at phasic aspects of neurons, while the previous results looked at tonic aspects. See Hepp-Reymond (1988) for a review of earlier results that also found dF/dt to be in phasic aspects of neuronal activity. Cheney and Fetz (1980) report that pyramidal tract neurons are more likely to be tonic neurons, while phasic neurons are more likely to be interneurons. Our model speaks only to the tonic component of the MI population.

In area 5, we will concentrate on the population of shoulder-related neurons reported by Kalaska et al. (1990). The goal response of these neurons is significantly stronger than the load response, and the goal and load axes are uncorrelated. Our theory suggests an explanation for this.

2 The population vector

Georgopoulos et al. (1983) proposed the sinusoidal function

$$b_i + k_i \cos(\phi - \phi_i) \tag{1}$$

as a fit to the neural response function mentioned above, where ϕ_i is the preferred direction, b_i a baseline, and k_i a gain. They then proposed the *population vector* as a method of calculating movement direction precisely. Each cell contributes a vector with direction equal to its preferred direction and length equal to its firing rate. As long as the preferred directions (ϕ_i) are uniformly distributed and the baselines (b_i) and gains (k_i) are uncorrelated with the preferred direction, the vector sum constitutes an accurate and precise predictor of the movement direction (Georgopoulos et al. 1988). This also holds in three dimensions.

The population vector is not a representation; it is a means of extracting the value from a representation of direction in which each neuron has a firing rate based on (1). This representation can be modified to represent a vector instead of just a direction. A vector has both direction ϕ and magnitude r. If (1) is modified to include a magnitude term

$$b_i + k_i \cdot r \cos(\phi - \phi_i) \tag{2}$$

then the population vector still extracts ϕ correctly. The magnitude r can be extracted by subtracting b_i, dividing by k_i (so that each cell represents $r\cos(\phi - \phi_i)$), rectifying at 0, and integrating over all angles ϕ_i.

This extended representation supports vector arithmetic. In an earlier paper, we called this representation a *sinusoidal array* (Touretzky et al. 1993).

Most other models of the motor system that discuss the reaching task (Bullock and Grossberg 1988; Burnod et al. 1990, 1992a, b; Lee and Zipser 1993) use (2) for the neural activity, but the evidence for its preference over (1) has been weak until recently. Schwartz and Georgopoulos (1987) report a weak but linear relation to movement amplitude (distance travelled) along a cell's preferred direction. Kurata (1993) reports a covariance with amplitude in the premotor cortex, but only two amplitudes were used, and so the linearity of this function cannot be judged. In another two-amplitude task, Riehle and

Requin (1989) report that very few cells had firing rates related to movement amplitude during a delay period. However, three recent articles (Schwartz 1992, 1993; Fu et al. 1993) have demonstrated significant relations to magnitude components in the motor and premotor cortices. Schwartz (1992, 1993) reports that the length of the population vector shows a significant correlation to speed in a tracing task, and that the maximal individual neuronal covariance with speed occurs in the cell's preferred direction. Using a reaching task with six different movement amplitudes, Fu et al. (1993) found that amplitude is a significant factor in neuronal firing, with a large linear component. They also state that the interaction terms between amplitude and direction are significant, and they suggest that in the interaction term, distance may be a gain parameter that multiplies the cosine of the direction.

Even if individual neurons do not respond linearly to r, but instead follow (1), it is still possible to obtain an ensemble linear response by assigning cells with the same preferred direction a variety of recruitment thresholds. Evarts et al. (1983) report that cells with higher thresholds are recruited at higher forces. But the large linear range of the motor cortical neurons described by Cheney and Fetz (1980) and the recent results from Fu et al. (1993) would seem to obviate the need for such a mechanism. Either way, because cells have minimal and maximal firing rates, a recruitment encoding is translatable to a linear response and vice versa.

Because the cosine function multiplied by the length of the vector is precisely the projection or inner (dot) product function, this encoding is not limited to two dimensions. It is extendable to n-dimensional vectors, and so can be used for 3-dimensional motor tasks.

3 Mathematical foundations

For each cell i, we define a preferred vector (in polar coordinates) $\vec{\tau}_i = (k_i, \phi_i)$. Then, with $\vec{v} = (r, \phi)$ the vector being represented, and $P_{\vec{v}}$ the population representation of $\vec{v}$, the firing rate of neuron i is

$$F(P_{\vec{v}}, i) = b_i + \vec{v} \cdot \vec{\tau}_i \tag{3}$$

where the dot denotes inner product.

As noted above, the distributed dot product encoding supports vector arithmetic. We can represent the vector quantity $\vec{v}_3 = \vec{v}_1 + \vec{v}_2$ as a population of cells in which each cell fires at the rate

$$F(P_{\vec{v}_3}, i) = b_i + (\vec{v}_1 + \vec{v}_2) \cdot \vec{\tau}_i \tag{4}$$

or because dot product distributes over addition,

$$F(P_{\vec{v}_3}, i) = b_i + \vec{v}_1 \cdot \vec{\tau}_i + \vec{v}_2 \cdot \vec{\tau}_i \tag{5}$$

Because the preferred directions of cells are randomly distributed throughout 360°, it is unlikely that in the separate representations of $\vec{v}_1$, $\vec{v}_2$, and $\vec{v}_3$, there will be exact matches for each preferred direction. Therefore, we approximate (5) by a symmetric distribution around $\vec{\tau}_i$.

The probability of a neuron in P_1 or P_2 making synaptic contact with a particular neuron in P_3 (where (P_1, P_2, and P_3 represent $\vec{v}_1$, $\vec{v}_2$, and $\vec{v}_3$, respectively) must be inversely related to the angle between their preferred directions, with 0° giving the highest probability of contact and 180° the lowest. We use a gaussian relation in our simulations, based on our observation of Kalaska et al. (1989, Fig. 9).[1]

Each population P_1 and P_2 contributes to the sum P_3 a bias factor equal to the average baseline $B = \frac{1}{n}\sum_{i=1}^{n} b_i$, thus contributing $2B$ together. But each neuron in P_3 should have a baseline rate of just B, so we must give P_3 neurons a bias term of $-B$. If the connection strengths are weighted by W_{13} and W_{23} (weighting connections from $P_1 \rightarrow P_3$ and $P_2 \rightarrow P_3$, respectively), the bias term must be $-\mathscr{B} = -(W_{13} + W_{23} - 1)B$.

Vector subtraction is equivalent to addition of a negated vector. Negation is in turn equivalent to a 180° rotation, so the subtraction $\vec{v}_3 = \vec{v}_1 + (-\vec{v}_2)$ can be performed by inverting the probability of P_2 neurons synapsing onto P_3 neurons, i.e. a difference of preferred directions of 180° should yield the highest probability of a connection.

Result of computer simulations of an earlier, more restricted formulation of this representation are described in Touretzky et al. (1993). New computer simulations are discussed in Sects. 5 and 6.

4 The loaded reaching task

Because the load axes of the MI neurons recorded in Kalaska et al. (1989) are approximately anti-correlated with their goal axes, these cells can be interpreted as contributing to a population of cells performing vector subtraction using the mechanism described in the previous section. We call this population performing vector subtraction P_M.[2] Because the relation of (tonic pyramidal) MI neurons to static force is sigmoidal with a large linear range, we suggest that force is the magnitude component of P_M.

In order to perform a vector subtraction, there must be two input signals: a goal signal and a load signal.[3] In our model, we place these two signals in two populations P_G and P_L (Fig. 2).

---

[1] Although this connection structure has not been observed *between* neuronal populations, a connection structure that is a function of preferred directions has been observed *within* a neuronal population (Georgopoulos et al. 1993).

[2] Although it is not necessary that these populations be in different cortical areas, only that they not share component neurons, for simplicity we will locate them in separate cortical areas. Certainly there are cells in MI which do not contribute to P_M. Only 41% of cells in MI show a correlation to static load (Werner et al. 1991). Similarly, there are cells in other cortical areas which could contribute to P_M. For example, 26% of cells in PMd show a response to load, and in some areas (notably PTNs and their neighbors) the proportion approaches the 41% seen in MI (Werner et al. 1991). All we are suggesting is that the cells recorded by proportion approaches the 41% seen in MI (Werner et al. 1991). All we are suggesting is that the cells recorded by Kalaska et al. (1989) contribute to the population P_M. Analogous qualifications apply to P_G (PMd) and $P_{G,L}$ (area 5).

[3] Both $\vec{G}$ and $\vec{L}$ will be transformed by interaction torques (Hollerbach and Flash 1982), so the vector subtraction must be performed after both vectors have been transformed into their shoulder effects.

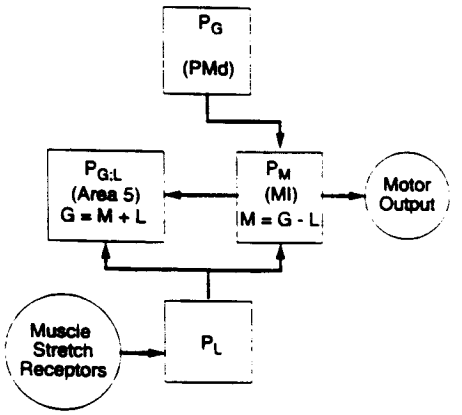

Fig. 2. Our mapping between populations and vectors required by the loaded reaching task

Because there is a population of shoulder-related neurons in PMd that do not show an individual load response but do show a cosine response to target direction, we place this population in P_G. As mentioned above, these PMd neurons tend to show a change in activity prior to either MI or area 5. Initial accleration, initial speed, amplitude of movement, and force are all linearly correlated (Flash and Hogan 1985), so no matter which quantity forms the magnitude component of P_G, the magnitude component of P_M can be force.

We know of no neuronal recordings that identify members of P_L (i.e. neurons showing only a load response), and we offer the existence of such neurons as a prediction of our theory.

We also propose that the population of area 5 cells recorded in Kalaska et al. (1990) are members of a population $P_{G:L}$ performing the vector addition $\vec{M} + \vec{L}$ (Fig. 2). Because $\vec{M} = \vec{G} - \vec{L}$, the two $\vec{L}$ components should cancel. If the spread to the input distributions [standard deviation σ of the gaussian in (7) below] were 0, then the two $\vec{L}$ components would balance exactly, and individual neurons would not show a load response. But because the input to each neuron in $P_{G:L}$ is a finite random selection from two gaussian distributions, the probability is small that every component of the load signal from the corollary discharge from P_M will be exactly balanced by the load signal from P_L. The two load signals do not exactly cancel out, predicting a small (but non-zero) individual load response uncorrelated with the neuron's goal axis. This was observed in Kalaska et al. (1990).

5 Details of the simulations

Our simulations use a simple integrate and fire neuron model. Each cell has a resting potential of 0 and a threshold θ_i. (The threshold varies from cell to cell but is assumed to have a gaussian distribution around 1 with a variance of 0.5.)

The cell integrates synaptic input linearly over time, and when the internal sum passes threshold, it fires a spike. A spike lasts for one time step, after which the cell enters a refractory state, modeled by a higher threshold which decays exponentially over time until the threshold returns to normal. That is

$$\theta_i = \theta_i^m + \theta_i^R \cdot \exp(-\tau_\theta \cdot t_s) \tag{6}$$

where θ_i^m is a minimum threshold, and θ_i^R is a refraction term, so that the maximum threshold for cell i is $\theta_i^m + \theta_i^R$. The constant τ_θ controls the rate of decay, and t_s is the amount of time since the most recent spike. During the refractory period, cells continue to integrate inputs. If the internal sum surpasses the high threshold, the cell spikes and starts a new refractory cycle. We add noise to a cell by adding or subtracting a percentage of the average baseline B to its activation at each time step.

Each population is made up of a number of cells (in our case 1500, see Table 1)[4] with preferred directions scattered randomly through 360° and baseline and gain parameters randomly chosen within a guassian (using the *polar method*, see Knuth 1969, pp. 104, 113) so as to fit the known data (Schwartz et al. 1988; Fig. 3). We force b_i and k_i to be ≥ 1, but we do not constrain them to be integral. Some neurons do have $k > b$ (Schwartz et al. 1988). For such neurons, $b_i + k_i \cdot r\cos(\phi - \phi_i) < 0$ for certain ϕ. Our abstract pyramidal cell naturally rectifies the firing rate to 0. The rectified cosine function is an approximation to a true cosine function, and if the ratio k/b is not too large, then the vector arithmetic computations still produce good results.

In our simulations, populations can play one of two roles. *Input populations* are assumed to fire spikes with a frequency equal to $F(P_i, i)$ in (3). This is simulated by adding $F(P_i, i) \cdot \Delta t$ to each cell's internal sum each time cycle. A cell spikes when it passes threshold. Cells in input populations refract as described above.

Summation populations take synaptic input from two other populations, which can be of either type. If cell i is in a population that forms an input to the summation population, and cell j is in the summation population, then the probability of cell i forming a synapse onto cell j is

$$G(\Delta\phi_{ij}) = \kappa \cdot \exp(-(\Delta\phi_{ij} - \mu)^2/\sigma^2) \tag{7}$$

where κ and σ are constants, $\Delta\phi_{ij}$ is the angle between ϕ_i and ϕ_j and $G(\Delta\phi_{ij})$ has a gaussian distribution.

For vector addition, the peak μ of $G(\Delta\phi_{ij})$ for both input populations is at $\Delta\phi_{ij} = 0°$; for vector subtraction, the peak for the minuend is at 0°, while the peak for the subtrahend is at 180°.

In order to implement the necessary bias factor $-\mathscr{B}$, at every clock cycle the net activation of each cell in the summation population is decreased by $\mathscr{B} \cdot \Delta t$. If a population forming an input to a summation population is

[4] We require such a large number of neurons in order to both achieve a high accuracy and replicate the distribution of b and k found in MI (Schwartz et al. 1988). If this constraint is relaxed, the model is accurate with only a few hundred neurons.

Table 1. Simulation parameters

Cell parameters:	
Number of cells in a population	1500
Mean baseline (b_i)	10 spikes/s
Baseline variance	10 spikes/s
Minimum baseline	1 spike/s
Mean gain (k_i)	8 spikes/s
Gain variance	8 spikes/s
Minimum gain	1 spike/s
Correlation between gain and baseline	0.9
Mean threshold (θ_i)	1
Threshold variance	0.5
Minimum threshold	0.1
Theta fall-off [τ_θ, (6)]	0.001
Noise	5%
Time step (Δt)	0.1 ms
Minimum spike rate	0 spikes/s
Maximum spike rate	100 spikes/s
Connection parameters:	
Connection probability [κ, (7)]	1.0
Connection variance [σ, (7)] ($P_G \rightarrow P_M$)	2.5 rad
Connection variance [σ, (7)] ($P_L \rightarrow P_M$)	2.5 rad
Connection variance [σ, (7)] ($P_M \rightarrow P_{G:L}$)	0.125 rad
Connection variance [σ, (7)] ($P_L \rightarrow P_{G:L}$)	0.125 rad
Connection weight ($W_{G\rightarrow M}$)	2
Connection weight ($W_{L\rightarrow M}$)	2
Connection weight ($W_{M\rightarrow G:L}$)	3.2
Connection weight ($W_{L\rightarrow G:L}$)	1

weighted by W_m, then the weights of the incoming synapses are set to $W_m/|\mathcal{S}_m(j)|$ where $|\mathcal{S}_m(j)|$ is the size of the set of neurons synapsing from population m onto neuron j. We have not modeled synaptic or axonal delays.

In order to determine the represented vector $\vec{v}' = (r', \phi')$ [an approximation to $\vec{v} = (r, \phi)$], we calculate ϕ' using the vector hypothesis (Georgopoulos et al. 1988), and r' by rectification and integration. We rectify the wave by subtracting the average baseline B from each neuron's frequency (calculated by averaging interspike intervals), divide by the average gain $K = \frac{1}{n}\sum_{i=1}^{n} k_i$, integrate over all neurons, and divide by one-half the number of neurons in the population. This is an approximation to the integral of half of the cosine wave, which is r'.

Our results show that vector addition and subtraction can be performed by spiking neurons very quickly. There is zero latency beyond transmission delays.

6 Results

Our simulations are designed to explore certain aspects of the theory diagrammed in Fig. 2, specifically, whether we can match the results of Kalaska et al. (1989, 1990) that (a) the load axes vary from 180° off the goal response in the MI population, while in the population in area 5 load axes are uncorrelated with goal axes, and (b) the average load response of the area 5 cells is smaller than the average goal response of those cells, while the magnitudes of the load and goal responses of the MI cells differ less. All of the simulations were run using the parameters in Table 1, chosen to match the data of Schwartz et al. (1988), see Fig. 3. We should point out, though, that the proposed architecture is quite robust and gives good accuracy and precision over a large range of parameter values.

6.1 Load axes and preferred goal directions

The observation that not all load and goal axes in the MI population recorded by Kalaska et al. (1989) differ by exactly 180° is explainable by sampling effects in the connection pattern between two populations. If the connection pattern is stochastic, then the input selection will not be entirely balanced around 180°. Any combination of high variance σ and low connection probability κ will produce results like that of Kalaska et al. (1989). In the Appendix, we give a method for determining the load and goal axes of a summation neuron in P_M given its connection matrix, and in this section we use the method to demonstrate the similarity between our simulations and the results of Kalaska et al.

The derived *goal axis*, γ_j of a summation neuron j receiving input from P_G and P_L is defined as the preferred vector when $\vec{L} = 0$. See the Appendix for the derivation $\mathcal{S}_G(j)$ is the input population to cell j from P_G.

$$\vec{\gamma}_j = \sum_{i \in \mathcal{S}_G(j)} w_{ij}^G \cdot \vec{\tau}_i \tag{8}$$

The derived *load axis* λ_j is defined as the preferred vector when $\vec{G} = 0$. It is calculated by analogy to γ_j

$$\vec{\lambda}_j = \sum_{i \in \mathcal{S}_L(j)} w_{ij}^L \cdot \vec{\tau}_i \tag{9}$$

If one rotates the load axes so that their corresponding goal axes are at 0°, one can see the approximate anti-correlation of the goal and load axes. This is the information contained in Fig. 9 of Kalaska et al. (1989). Our Fig. 4 compares our simulation results with the data reported in that figure.

One can calculate $\vec{\lambda}_j$ for cell j in $P_{G:L}$ by summing the contributions from $\vec{\lambda}_i$ for cells in P_M and $\vec{\tau}_i$ for cells in P_L that synapse onto cell j. $\vec{\gamma}_j$ for cell j in $P_{G:L}$ can be calculated from the influence of $\vec{\gamma}_i$ for cells in P_M that synapse on cell j. Figure 5 compares our simulation results with the data reported in Kalaska et al. (1990).

6.2 Magnitudes of load and goal responses

A higher proportion of cells are sensitive to load in MI than in area 5 (Werner et al. 1991; Kalaska and Crammond 1992; Kalaska et al. 1992), and those cells that do respond to load in area 5 have a smaller response to load than cells in MI (Kalaska 1991). Our theory suggests that this is because the population of cells in area 5 recorded in Kalaska et al. (1990) are part of a population $P_{G:L}$ which is performing the calculation $\vec{M} + \vec{L}$, or since $\vec{M} = \vec{G} - \vec{L}$, that $P_{G:L}$ is calculating $(\vec{G} - \vec{L}) + \vec{L}$. A cell in $P_{G:L}$ will be sensitive to load if and only if the inputs

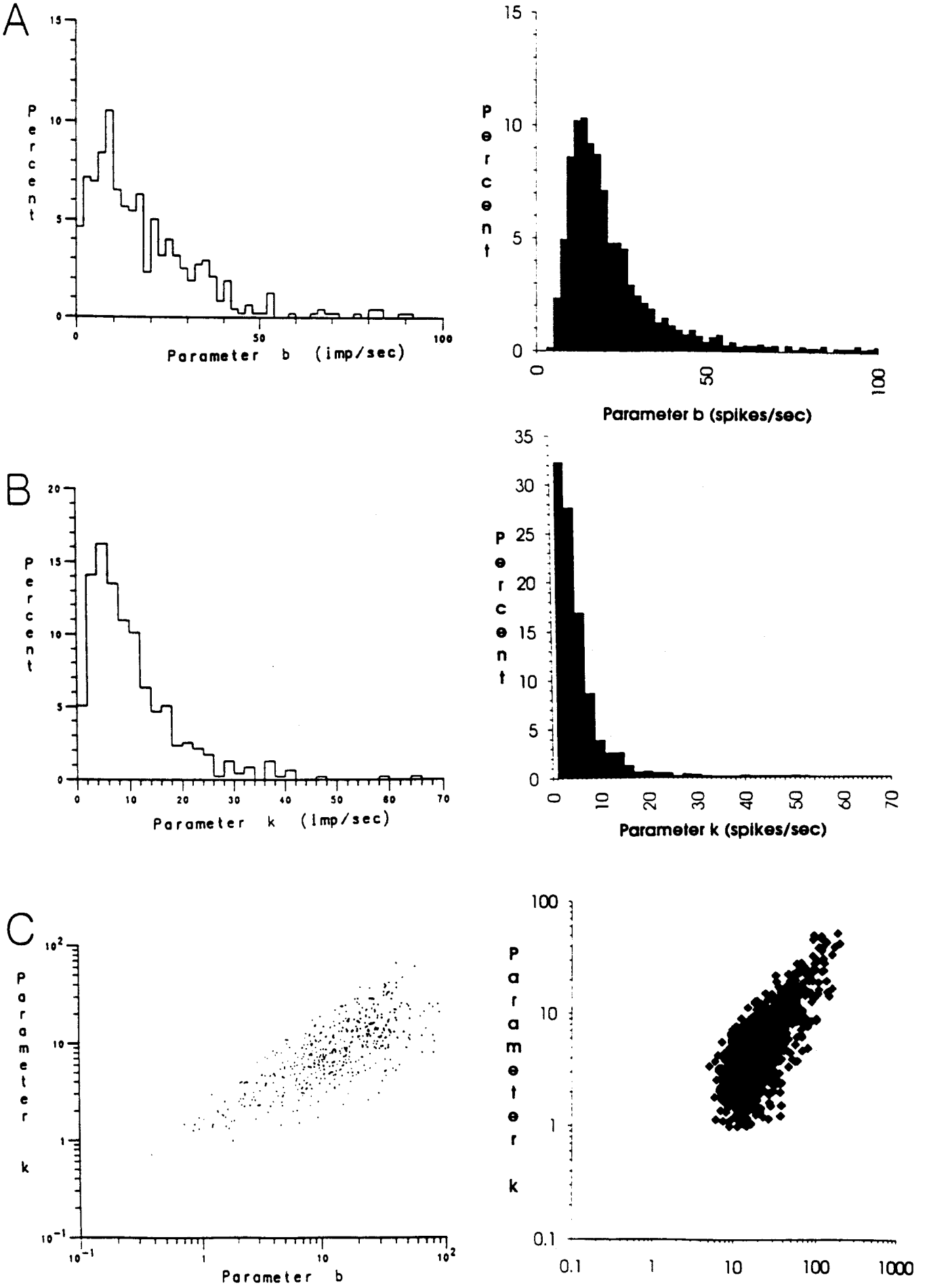
A
Percent
Parameter b (imp/sec)
Parameter b (spikes/sec)
B
Percent
Parameter k (imp/sec)
Parameter k (spikes/sec)
C
Parameter k
Parameter b
Parameter k

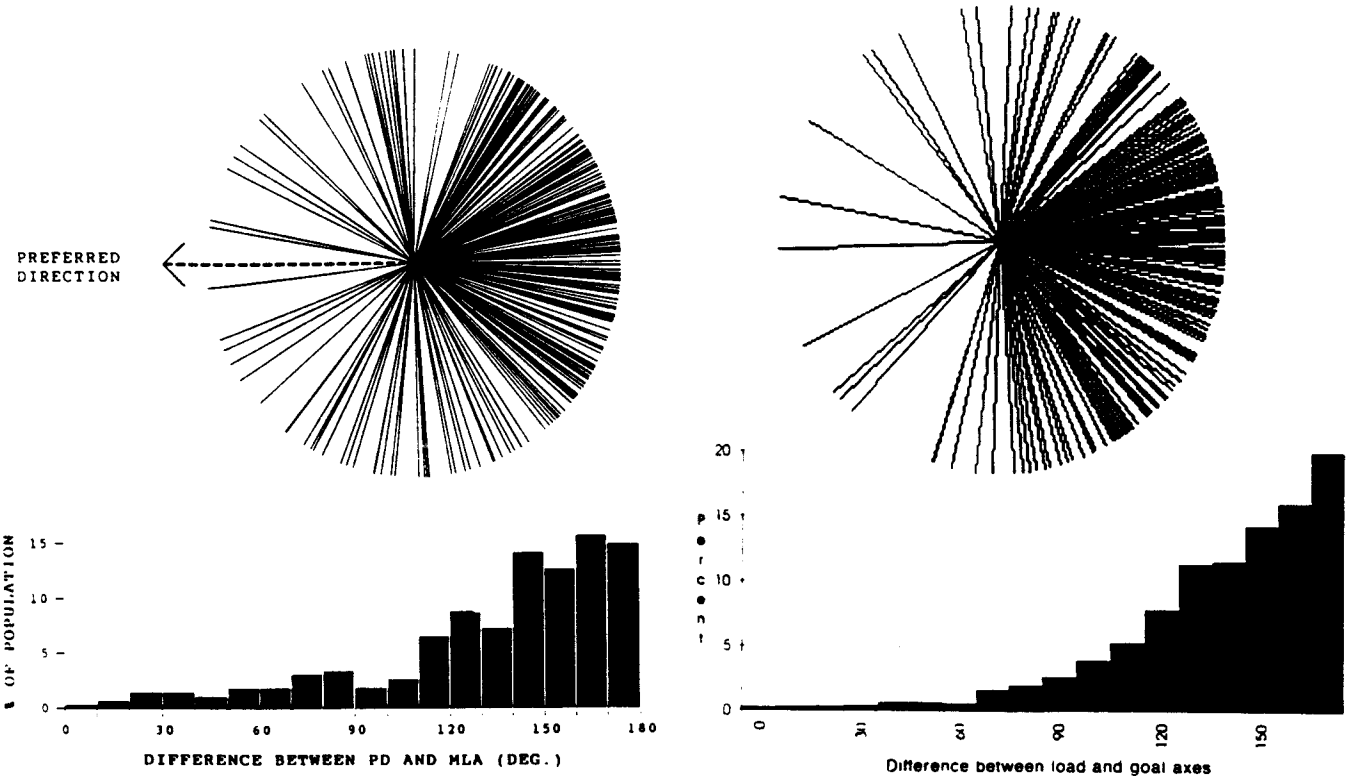

Fig. 4. Comparison of load axes with respect to goal axes for MI and P_M, showing distribution of angular difference between preferred directions (goal axis) and maximum response to load (load axis). *Left* data from Kalaska et al. (1989), used with permission of the author and publisher. *Right*, output of our simulations. Note that many cells have close to a 180° difference between goal and load axes, but for a significant percentage the difference is much lower. *Left*, 262 cells; *right*, 250 cells chosen randomly from 1500. *Right bar graph* is percentage over all 1500 cells

from P_L and the load component of the corollary discharge from P_M fail to cancel.

We can analytically determine the response of a cell to load or goal by examining the lengths of $\vec{\lambda}_j$ and $\vec{\gamma}_j$, respectively (not shown in Figs. 4 and 5), e.g., a cell with a long load axis has a stronger gain with respect to $\vec{L}$ and thus a stronger response to it.

In our simulations, we can adjust the weights of the connections between P_G and P_M, between P_M and $P_{G;L}$, as well as between P_L and P_M and P_L and $P_{G;L}$. We can also adjust the connection variance σ of the gaussian $G(\Delta\phi_{ij})$ for each of these connection matrices. There are not enough data to constrain a model with this many parameters, so we showed that our simulations perform accurate vector arithmetic over a wide range of parameters and chose a set of parameters that replicated the data well.

As long as the strength of the load input from the corollary discharge from P_M and that of the load input from P_L into $P_{G;L}$ are equal, the two loads will balance, and the average response to load from $P_{G;L}$ neurons will be small. On the other hand, because there is no negative $\vec{G}$ to counter-balance the $\vec{G}$ signal transmitted through the corollary discharge from P_M, the neuronal response of $P_{G,L}$ neurons to $\vec{G}$ will be of normal magnitude.

The parameters in Table 1 include small variances for the input connections $P_{G,L}$ to better balance the respon-ses to load from P_M and from P_L. The higher weight for the connection from P_M to $P_{G,L}$ is required because the negative load signal is diluted by passing through P_M.

We can see the differential response to $\vec{G}$ and $\vec{L}$ in $P_{G;L}$ across a wide range of parameters. Given the parameters in Table 1, our simulations show that the ratio between goal and load responses in P_M is 1:1, but in $P_{G;L}$ the ratio is 2.4:1. Although these results are a function of the parameters used, for a broad range of values for $W_{M\to G,L}$ and $W_{L\to G,L}$, the goal response in $P_{G,L}$ is larger than the load response.

6.3 *Varying parameters: robustness*

Although we report parameters in this paper tuned to match the biological data (see Fig. 3–5), our simulations showed fast, accurate, and precise answers over a large range of values. The parameters in Table 1 enable vector addition with an accuracy of better than $\pm 7.5\%$. The answers are most accurate when $B \gg K > 0$. When the connection probability [κ of the gaussian $G(\Delta\phi_{ij})$ in (7)] is higher or the connection variance (σ) is lower, the variation in the difference between load and goal axes in P_M is much less, and the accuracy of the vector arithmetic increases.

Fig. 3A–C. Comparison between baseline and gain distributions in data recorded from MI (568 cells, *left*) and P_M in our simulation (1500 cells, *right*). *Top*, comparison of b_i (baseline). *Middle*, distribution of k_i (gain). *Bottom*, correlation of k_i and b_i. *Left-hand graphs* are from Schwartz et al. (1988), used with permission of the author and publisher

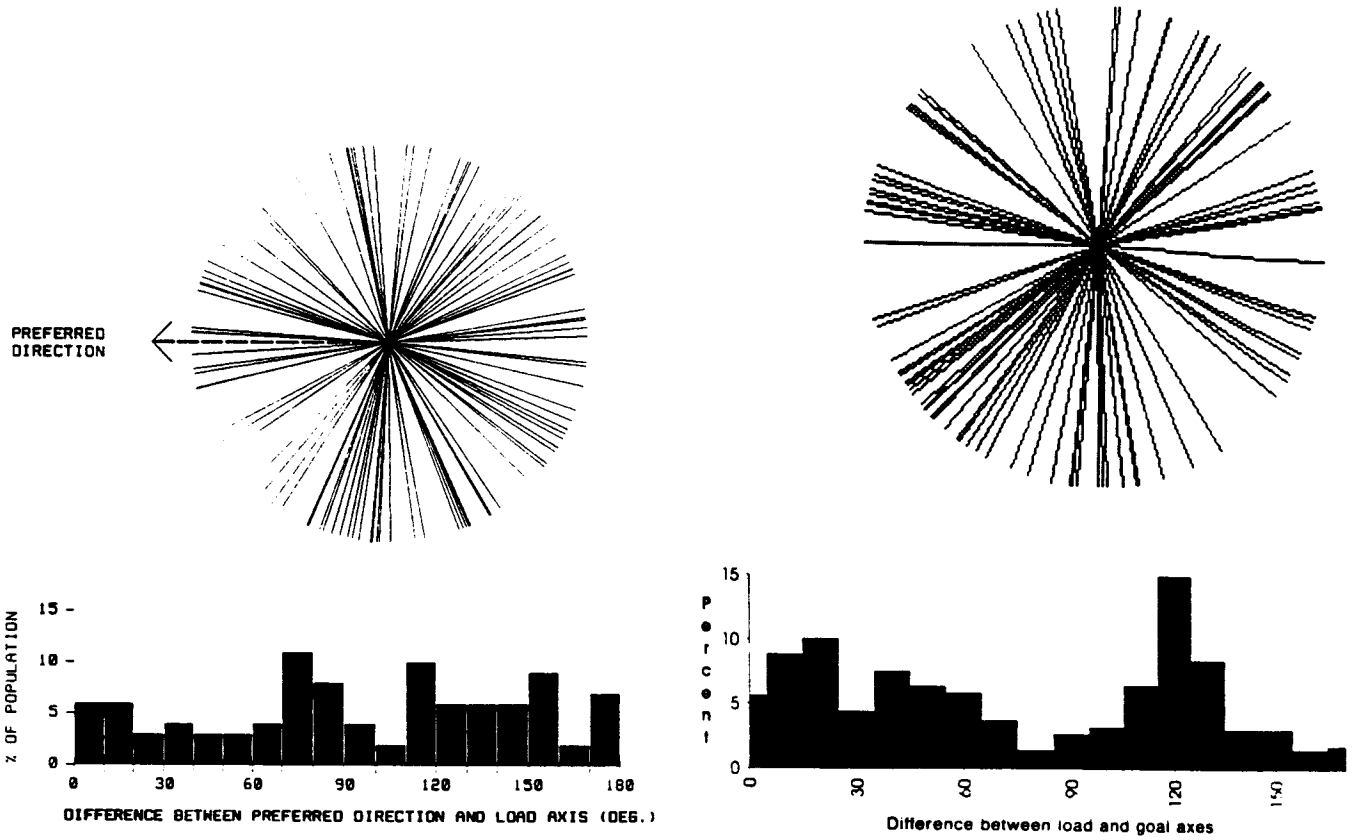

Fig. 5. Comparison of load axes with respect to goal axes for area 5 and $P_{G;L}$. *Left*, data from Kalaska et al. (1990), used with permission of the author and publisher. *Right*, output of our simulations. *Left*, 100 cells; *right*, 100 cells chosen randomly from 1500. *Right bar graph* is percentage over all 1500 cells

7 Other interpretations

7.1 MI: interaction torques

Flash and Mussa-Ivaldi (1990) have shown that the stiffness of the human arm is not equal in all directions, but rather that it is stronger along the axis passing through the hand and shoulder than perpendicular to this axis. Kalaska et al. (1989) do, in fact, report that the length of the population vector in MI compensating for the load is shorter when compensating for loads towards and away from the body than when compensating for side-to-side loads. In our model we do not require $\bar{L}$ to be defined by the external load, but by the load felt at the shoulder. (The recordings are in shoulder-controlling populations.)

Hollerbach and Flash (1982) demonstrate that because of interaction torques between the elbow and shoulder joints, forces opposing at the hand are not necessarily opposing at the shoulder. It is possible, therefore, that the reason the load and goal axes in the MI population do not differ by exactly 180° is because the load-countering and hand-motion effects of the muscle units they innervate do not exactly differ by 180°.

If this is the biological reason, then it is still possible to interpret the response functions of MI neurons as a vector subtraction using distributed dot products, but the use of this interpretation becomes questionable.

We can design an experiment to differentiate these hypotheses. If only one joint is involved in the experiment, then the load and goal vectors are directly opposite. If the spread of the distribution of load and goal axes reported by Kalaska et al. is due entirely to interaction torques, it should disappear.

What advantage could there be in such a spread? Because the number of neurons synapsing on a summation neuron increases monotonically as σ (7) increases, allowing a non-zero spread expands the input population and improves the frequency summation properties of the summation neuron. Essentially, a non-zero σ allows the summation neuron to use the law of large numbers to average out discretization effects in its input.

In a one-dimensional elbow experiment, recording from SMA, MI, and putamen, Crutcher and Alexander (1990) report three classes of neurons: 'directional', 'muscle-like', and 'other'. *Directional* cells were defined as those which showed a preference for flexion or for extension but did not show a relation to loads; *muscle-like* cells showed a preference for direction and for loads opposite to their direction; *other* cells were those which showed a preference for direction and for load assisting movements in their preferred direction. Although interpreting

the timing results from these experiments is beyond the scope of this paper, *directional* cells could either truly have no load response or their load axes could be perpendicular to their preferred directions. *Muscle-like* cells could be explained by load axes opposite their preferred directions, and *other* cells by load axes parallel to their preferred directions. Our model shows that this third class of cells does not have to be interpreted as anomalous; they could be generated by the same connectivity distribution as the other two classes.

7.2 Burnod et al.'s model

Caminiti and his colleagues have reported (1990a, b, 1991) that the encoding of the direction of arm movement (which we call $\vec{G}$) varies as a function of the rotation of the arm in shoulder-centered coordinates. Our theory is compatible with this: the subtraction we are proposing occurs after the rotation has been compensated for. In fact, their model (Burnod et al. 1990, 1992a, b) could be the source of $\vec{G}$ because their output representation has the required mathematical properties to be interpreted as a distributed dot product representation.

8 Predictions

In this section, we detail our predictions: that a population of neurons in arm-related areas of PMd will be found to be connected to another population of arm-related neurons in MI so that the synaptic efficacy is a function of the difference in preferred directions, that this second population will be found to be connected to a third population of arm-related cells in area 5 with a similar connection structure, and that a population representing the load signal $\vec{L}$ exists somewhere in the brain with connections to the arm-populations in MI and in area 5.

8.1 Connection functions

Georgopoulos et al. (1993) used timing difference distributions to determine the connection strength within a neu-ronal population in MI. They found that the probability of connection is inversely proportional to the similarity of the two preferred directions. Our model requires this property *between* neuronal populations, in particular, between P_L and P_M, between P_G and P_M, between P_L and $P_{G;L}$, and between P_M and $P_{G;L}$. We have identified neurons which could contribute to the populations P_G, P_M, and $P_{G;L}$, which makes this prediction directly testable.

8.2 P_L

The load vector $\vec{L}$ must be represented in some population of cells P_L. This population will have to be separated from P_M either in space or in time. Kalaska et al. (1989) report that during the center hold time, the cells show a strong load response, implying that the separation might be in time. Other possibilities include the thalamus, somatosensory cortices, or cerebellum. The motor stretch reflex is mediated through the motor cortex (a) directly, (b) via the cerebellum, and (c) via the somatosensory cortices. See Hepp-Reymond (1988) for a review. Fortier et al. (1989) have shown cosine response functions in the cerebellum.

9 Discussion: hierarchical vs parallel processing

An overly simplistic interpretation of our model is that the motor cortex computes a motion command by subtracting the load vector from the goal vector in a purely feed-forward process. We make no such claim. Cortical areas are typically reciprocally connected, and within an area there are many intrinsic connections which must play some role in processing. Whether the primate motor system is primarily hierarchical or heterarchical in nature is as yet unreasolved. See Alexander et al. (1992), Fetz (1992), Johnson (1992), Kalaska et al. (1992), Kalaska and Crammond (1992) for reviews of this issue.

Although our paper talks in terms of cells 'performing' specific arithmetic operations such as $\vec{M} \Leftarrow \vec{G} - \vec{L}$, all we are really claiming is that a vector arithmetic relationship holds among certain populations. The causal basis for this relationship need not be nearly as simple as the feed-forward circuitry used in our simulations. However, the preferred directions of cells within a population representing a vector quantity must in some way determine their connectivity with cells in other such populations.

We have offered a way of interpreting cell responses in MI and area 5 in terms of vector arithmetic relations. Cells with cosine responses in the reaching task have been found throughout the motor system (PMd: Caminiti et al. 1990a, 1991; MI: Schwartz et al. 1988; area 5: Kalaska et al. 1989; cerebellum: Fortier et al. 1989). Vector arithmetic would be useful in many aspects of movement and cognition.

Acknowledgements Hank Wan contributed to early work on this paper. Dr. John Kalaska provided helpful comments on earlier drafts and on early versions of this work, and permission to use the illustrations in Figs. 1, 4, and 5. We would also like to thank Dr. Apostolos Georgopoulos for comments on our work, and for permission to reproduce the graphs in Fig. 3. We thank Dr. Steven Wise for helpful discussions. We also thank two anonymous reviewers for helpful comments. This work was supported in part by a grant from the Fujitsu Corporation. David Redish was supported by an NSF fellowship.

Appendix

In this section, we derive the analytical equation for the goal axis γ_j for P_M summation neurons. The equations for the load axis λ_j for P_M neurons and for γ_j and λ_j for $P_{G;L}$ neurons are analogous.

In order to simplify the following equations, we define $w_{ij}^L = W_L/|\mathcal{S}_L(j)|$, where w_{ij}^L is the synaptic efficacy between cell i in P_L and cell j in P_M, W_L is the (constant) connection weight between populations P_L and P_M, and

$|\mathcal{S}_L(j)|$ is the cardinality of the set of cells in P_L synapsing on cell j. We define w_{ij}^G analogously. We also define $\mathcal{B} = (W_L + W_G - 1) \cdot B$.

Thus, we can write the frequency of neuron j in P_M as:

$$F(P_M, j) = -\mathcal{B} + \sum_{i \in \mathcal{S}_L(j)} w_{ij}^L \cdot F(P_L, i) + \sum_{i \in \mathcal{S}_G(j)} w_{ij}^G \cdot F(P_G, i) \quad (10)$$

and by substituting in (3)

$$F(P_M, j) = -\mathcal{B} + \sum_{i \in \mathcal{S}_L(j)} w_{ij}^L \cdot (b_i + \vec{\mathbf{L}} \cdot \vec{\tau}_i) + \sum_{i \in \mathcal{S}_G(j)} w_{ij}^G \cdot (b_i + \vec{\mathbf{G}} \cdot \vec{\tau}_i) \quad (11)$$

We can transform this equation by splitting the summations:

$$F(P_M, j) = -\mathcal{B} + \sum_{i \in \mathcal{S}_L(j)} w_{ij}^L \cdot b_i + \sum_{i \in \mathcal{S}_G(j)} w_{ij}^G \cdot b_i + \sum_{i \in \mathcal{S}_L(j)} w_{ij}^L \cdot \vec{\mathbf{L}} \cdot \vec{\tau}_i + \sum_{i \in \mathcal{S}_G(j)} w_{ij}^G \cdot \vec{\mathbf{G}} \cdot \vec{\tau}_i \quad (12)$$

By (3):

$$F(P_M, j) = b_j + \vec{\mathbf{M}} \cdot \vec{\tau}_j \quad (13)$$

Thus, by substitution, we have

$$b_j + \vec{\mathbf{M}} \cdot \vec{\tau}_j = -\mathcal{B} + \sum_{i \in \mathcal{S}_L(j)} w_{ij}^L \cdot b_i + \sum_{i \in \mathcal{S}_G(j)} w_{ij}^G \cdot b_i + \sum_{i \in \mathcal{S}_L(j)} w_{ij}^L \cdot \vec{\mathbf{L}} \cdot \vec{\tau}_i + \sum_{i \in \mathcal{S}_G(j)} w_{ij}^G \cdot \vec{\mathbf{G}} \cdot \vec{\tau}_i \quad (14)$$

When $\vec{\mathbf{L}}$, $\vec{\mathbf{G}}$, and $\vec{\mathbf{M}}$ are all zero, we get

$$b_j = -\mathcal{B} + \sum_{i \in \mathcal{S}_L(j)} w_{ij}^L \cdot b_i + \sum_{i \in \mathcal{S}_G(j)} w_{ij}^G \cdot b_i \quad (15)$$

Because b_j is a constant, this gives the value for b_j even when the vectors are non-zero. We can subtract b_j from (14) to get

$$\vec{\mathbf{M}} \cdot \vec{\tau}_j = \sum_{i \in \mathcal{S}_L(j)} w_{ij}^L \cdot \vec{\mathbf{L}} \cdot \vec{\tau}_i + \sum_{i \in \mathcal{S}_G(j)} w_{ij}^G \cdot \vec{\mathbf{G}} \cdot \vec{\tau}_i \quad (16)$$

The *goal axis*, γ_j, is defined as the preferred vector when $\vec{\mathbf{L}} = 0$. When $\vec{\mathbf{L}} = 0$, the summation based on its dot product is also 0, and we get

$$\vec{\mathbf{M}} \cdot \vec{\gamma}_j = \sum_{i \in \mathcal{S}_G(j)} w_{ij}^G \cdot \vec{\mathbf{G}} \cdot \vec{\tau}_i \quad (17)$$

or

$$\vec{\mathbf{M}} \cdot \vec{\gamma}_j = \vec{\mathbf{G}} \cdot \sum_{i \in \mathcal{S}_G(j)} w_{ij}^G \cdot \vec{\tau}_i \quad (18)$$

Since $\vec{\mathbf{M}} = \vec{\mathbf{G}}$ when $\vec{\mathbf{L}} = 0$, we have

$$\vec{\gamma}_j = \sum_{i \in \mathcal{S}_G(j)} w_{ij}^G \cdot \vec{\tau}_i \quad (19)$$

In other words, the goal axis of a P_M summation neuron is the weighted average of the preferred vectors of its input population from P_G.

References

Alexander GE, DeLong MR, Crutcher M (1992) Do cortical and basal ganglionic motor areas use 'motor programs' to control movement? Behav Brain Sci 15:656–665

Bullock D, Grossberg S (1988) Neural dynamics of planned arm movements: emergent invariants and speed-accuracy properties during trajectory formation. Psychol Rev 95:49–90

Burnod Y, Caminiti R, Johnson P, Grandguillaume P, Otto I (1990) Model of visuomotor transformations performed by the cerebral cortex to command arm movements at visual targets in the 3-d space. In: Eckmiller R (ed) Advanced neural computers. Elsevier, New York, pp 33–41

Burnod Y, Grandguillaume P, Otto I, Ferraina S, Johnson P, Caminiti R (1992a) Visuomotor transformations underlying arm movements toward visual targets: a neural network model of cerebral cortical operations. J Neurosci 12:1435–1453

Burnod Y, Grandguillaume, P, Otto I, Johnson P, Caminiti R (1992b) Reaching toward visual targets. ii. Computational studies. In: Caminiti R, Johnson P, Burnod Y (eds) Control of arm movement in space. Experimental brain research, vol 22. Springer Berlin Heidelberg New York, pp 159–174

Caminiti R, Johnson P, Burnod Y, Galli C, Ferraina S (1990a) Shift of preferred directions of premotor cortical cells with arm movements performed across the workspace. Exp Brain Res 83:228–232

Caminiti R, Johnson P, Urbano A (1990b) Making arm movements within different parts of space: dynamic aspects in the primate motor cortex. J Neurosci 10:2039–2058

Caminiti R, Johnson P, Galli C, Ferraina S, Burnod Y (1991) Making arm movements within different parts of space: the premotor and motor cortical representation of a coordinate system for reaching to visual targets. J Neurosci 11:1182–1197

Cheney P, Fetz E (1980) Functional classes of primate corticomotoneuronal cells and their relation to active force. J Neurophysiol 44:773–791

Crutcher MD, Alexander GE (1990) Movement-related neuronal activity selectively coding either direction or muscle pattern in three motor areas of the monkey. J Neurophysiol 64:151–163

Evarts EV, Fromm C, Kroller J, Jennings VA (1983) Motor cortex control of finely graded forces. J Neurophysiol 49:199–1215.

Fetz E (1992) Are movement parameters recognizably coded in the activity of single neurons? Behav Brain Sci 15:679–690

Flash T, Hogan N (1985) The coordination of arm movements: an experimentally confirmed mathematical model J Neurophysiol 5:1688–1703

Flash T, Mussa-Ivaldi F (1990) Human arm stiffness characteristics during the maintenance of posture. Exp Brain Res 82:315–326

Fortier P, Kalaska J, Smith A (1989) Cerebellar neuronal activity related to whole-arm reaching movements in the monkey. J Neuro-physiol 62:198–211

Fu Q, Suarez J, Ebner T (1993) Neuronal specification of direction and distance during reaching movements in the superior precentral premotor area and primary motor cortex of monkeys. J Neurophysiol 70:2097–2116

Georgopoulos A, Caminiti R, Kalaska J, Massey J (1983) Spatial coding of movement: a hypothesis concerning the coding of movement direction by motor cortical populations. Exp Brain Res (Suppl) 7:327–336

Georgopoulos A, Kettner R, Schwartz A (1988) Primate motor cortex and free arm movements to visual targets in three-dimensional space. ii. Coding of the direction of movement by a neuronal population. J Neurosci 8:2928–2937

Georgopoulos A, Ashe J, Smyrnis N, Taira M (1992) The motor cortex and the coding of force. Science 256:1692–1695

Georgopoulos A, Taira M, Lukashin A (1993) Cognitive neurophysiology of the motor cortex. Science 260:47–52

Hepp-Reymond M (1988) Functional organization of motor cortex and its participation in voluntary movements. In: Steklis H, Erwin J (eds) Neurosciences (Comparative Primate Biology, Vol 4) Liss, New York

Hollerbach JM, Flash T (1982) Dynamic interactions between limb segments during planar arm movement. Biol Cybern 44:67–77

Johnson P (1992) Toward an understanding of the cerebral cortex and reaching movements: a review of recent approaches. In: Caminiti R, Johnson P, Burnod Y (eds) Control of arm movement in space. Experimental Brain Research, vol 22. Springer, Berlin Heidelberg New York, pp 199–262

Kalaska J (1991) What parameters of reaching are encoded by discharges of cortical cells? In: Humphrey D, Freund HJ (eds) Motor control: concepts and issues. Wiley, New York, pp 307–330

Kalaska J, Crammond D (1992) Cerebral cortical mechanisms of reaching movements. Science 255:1517–1523

Kalaska J, Cohen D, Hyde M, Prud'homme M (1989) A comparison of movement direction-related versus load direction-related activity in primate motor cortex, using a two-dimensional reaching task. J Neurosci 9:2080–2102

Kalaska J, Cohen D, Prud'homme M, Hyde M (1990) Parietal area 5 neuronal activity encodes movement kinematics not movement dynamics. Exp Brain Res 80:351–364

Kalaska J, Crammond D, Cohen D, Prud'homme M, Hyde M (1992) Comparison of cell discharge in motor, premotor, and parietal cortex during reaching. In: Caminiti R, Johnson P, Burnod Y (eds) Control of arm movement in space. Experimental Brain Research, vol 22. Springer, Berlin Heidelberg New York, pp 129–146

Knuth D (1969) The art of computer programming: seminumerical algorithms, Vol 2. Addison-Wesley, Reading, Mass

Kurata K (1993) Premotor cortex of monkeys: set- and movement-related activity reflecting amplitude and direction of wrist movements. J Neurophysiol 69:187–200

Lee SJ, Zipser D (1993) A network model of direction tuning and mental rotation. Soc Neurosci Abstr 19:1207

Riehle A, Requin J (1989) Monkey primary motor and premotor cortex: single-cell activity related to prior information about direction and extent of an intended movement. J Neurophysiol 3:534–549

Schwartz A, Georgopoulos A (1987) Relations between the amplitude of 2-dimensional arm movements and single cell discharge in primate motor cortex. Soc Neurosci Abstr 13:244

Schwartz A, Kettner R, Georgopoulos A (1988) Primate motor cortex and free arm movements to visual targets in three-dimensional space. i. Relations between single cell discharge and direction of movement. J Neurophysiol 8:2913–2927

Schwartz A (1992) Motor cortical activity during drawing movements: single-unit activity during sinusoid tracing. J Neurophysiol 68:528–541

Schwartz A (1993) Motor cortical activity during drawing movements: population representation during sinusoid tracing. J Neurophysiol 70:28–36

Touretzky D, Redish AD, Wan H (1993) Neural representation of space using sinusoidal arrays. Neural Comput 5:869–884

Werner W, Bauswein E, Fromm C (1991) Static firing rates of premotor and primary motor cortical neurons associated with torque and joint position. Exp Brain Res 86:293–302

Wise SP (1993) Monkey motor cortex: movements, muscles, motoneurons and metrics. Trends Neurosci 16:46–49